Available online at www.sciencedirect.com
SCIENCE DIRECT®
Journal of Theoretical Biology 234 (2005) 311–327
Journal of Theoretical Biology
www.elsevier.com/locate/yjtbi

The complex effect of granulocyte colony-stimulating factor on human granulopoiesis analyzed by a new physiologically-based mathematical model

V. Vainstein[a,*], Y. Ginosar[a,1], M. Shoham[b], D.O. Ranmar[a], A. Ianovski[b], Z. Agur[a,b]

[a]*Institute for Medical Biomathematics, POB 282, Hagteena St. 10, Bene-Ataroth 60991, Israel*
[b]*Optimata Ltd., 11, Tuval St., Ramat-Gan 52522, Israel*

Received 30 August 2004; received in revised form 12 November 2004; accepted 17 November 2004

Abstract

Neutropenia, frequently a side effect of chemo- and radiotherapy, increases susceptibility to microbial infections and is a life-threatening condition. For realistically predicting drug treatment effects on granulopoiesis, we have constructed a new mathematical model of granulopoiesis in the bone marrow and in the peripheral blood, featuring cell cycle phase transition and detailed granulocyte-colony stimulating factor (G-CSF) pharmacokinetics (PK) and pharmacodynamics (PD), including intracellular second messenger. Using this model, in conjunction with clinical results, we evaluated the system parameters, implemented those in the model and successfully retrieved the results of several independent clinical experiments under a wide range of G-CSF regimens. Our results show that the introduction of G-CSF-controlled intracellular second messenger is indispensable for precise retrieval of the clinical results, and suggest that the half-life of this messenger varies between a single and multiple G-CSF administration schedules. In addition, our model provided reliable steady-state, as well as dynamic, estimations of human granulopoiesis parameters. These included an estimation of apoptosis index in the post-mitotic compartment, which corroborates previous results. At present the model is used for suggesting improved drug regimens.

Keywords: Granulopoiesis; G-CSF; Mathematical model

1. Introduction

Formation of granulocytic leucocytes (also called polymorphonuclear cells—PMN, or neutrophils) from pluripotent hematopoietic stem cells in the adult bone marrow (BM) is denoted by Granulopoiesis (see detailed description in Hoffman, 2000). Granulopoiesis is initiated when pluripotent stem cells perform several steps of division and commitment, which are recognized phenotypically as transition through progenitor sub-compartments (CFU-GM, CFU-G). Granulocytic progenitors, originated from BM pluripotent stem cells, differentiate into precursor cells, which constitute three microscopically discernable sequential sub-compartments: myeloblasts (M_1), promyelocytes (M_2) and myelocytes (M_3). Still capable of proliferation, these three sub-compartments can be regarded as a mitotic compartment. During further differentiation myelocytes sequentially become metamyelocytes, band granulocytes, and segmented—fully mature—granulocytes (PMNs). As these cells cannot proliferate they can be regarded as one post-mitotic compartment (PMC). Post-mitotic granulocytes enter the peripheral blood and into the tissues, where they function as an antimicrobial shield.

One of the most important regulators of granulopoiesis is the hormone granulocyte-colony stimulating

*Corresponding author. Tel.: 972 3 9733075; fax: 972 3 9733410.
E-mail address: vladimir@imbm.org (V. Vainstein).
[1]Present address: Department of Mathematics, University of Haifa, Mount Carmel, Haifa 31905, Israel.

0022-5193/$ - see front matter © 2005 Elsevier Ltd. All rights reserved.
doi:10.1016/j.jtbi.2004.11.026

factor (G-CSF) (reviewed in Kuwabara et al., 1996a). It stimulates the proliferation of neutropenic progenitor cells, their differentiation into granulocytes, and accelerates the release of neutrophils from the PMC into the blood.

Recombinant human G-CSF (rhG-CSF) is used for therapy of neutropenia, which is one of the most frequent and dose-limiting side-effects of chemotherapy and radiotherapy (Rolston, 2000; Rahman et al., 1997). However, rhG-CSF clinical administration schedule is determined by an inefficient method of trial-and-error. In contrast, by carefully describing granulopoiesis in a mathematical model and implementing the model in the computer, one will be able to simulate granulopoiesis under different drug schedules in silico, and, subsequently, propose improved drug treatments, to be further validated in clinical trials.

Several mathematical models of granulopoiesis were proposed in the last decades. Rubinow and Leibowitz (1975) suggested a model, which includes proliferative and maturing compartments with a cell cycle structure. The control of proliferation and maturation rates was assumed to be mediated by a simplified negative feedback of the total number of cells in the lineage and the number of PMNs in the blood. This model does not allow for specific growth-factor effect (which were yet unknown) and, hence, cannot be employed for investigation of G-CSF-driven granulopoiesis.

Models of human granulopoiesis proposed in Fliedner et al. (1996) and Steinbach et al. (1980) are characterized by fractional proliferation and maturation rates. Proliferation rate depends on BM cellularity, while inflow from the BM to blood depends on granulocyte releasing factor (GRF—former name of G-CSF). GRF production rate depends on PMN count in blood, while clearance is fractional. The authors simulate the dynamics of post-radiation BM injury. Another model (Schmitz et al., 1990, 1993) resembles the previous ones, with two important distinctions: (a) proliferation rate depends on G-CSF; (b) de-margination of PMNs (transition from the marginal into circulating pool) is introduced as an additional G-CSF-dependent phenomenon. Using this model the authors were able to simulate the effect on PMN count of several days of treatment of G-CSF. Mackey (1997) proposed a general model of granulopoiesis with distributed delayed feedback of PMN count on inflow of cells from the BM into blood and no explicit description of different BM compartments. Stability analysis and cyclic neutropenia retrieval were successfully performed. Recently, granulopoiesis models have been put forward by Shochat et al. (2002) and Ostby et al. (2003), which were aimed at retrieving PMN blood count dynamics in patients who had undergone BM transplantation experiments.

For being clinically implementable, models of human granulopoiesis have to be evaluated by their ability to accurately retrieve several, independent, detailed experiments, such as de Haas et al. (1994) and Chatta et al. (1994). Moreover, having a potential effect on the overall dynamics, drugs' differential interaction with different cell-cycle phases should be taken account of in such models. As the aforementioned models do not allow for cell-cycle phase transition and detailed G-CSF dynamics they cannot satisfy these requirements and, therefore, cannot precise administration schedules of G-CSF and cell-cycle phase-specific chemotherapeutic agents.

The aim of the present work is to put forward a retrospectively validated granulopoiesis model to be used in clinical and pharmacological decision-making. To this end we first provide a detailed mathematical description of human granulopoiesis, including local and hormonal (G-CSF) feedback control.

Our new granulopoiesis model, incorporates most of available experimental information on granulopoiesis dynamics in man including G-CSF secretion, diffusion, clearance and interaction with different cell compartments. In order to increase its realism and prediction accuracy, we introduced in the model several new properties, which distinguish it from previously published models.

The model features explicit cell-cycle structure in the mitotic compartment and receptor-mediated G-CSF clearance with realistic experimentally-based values of receptor dynamics. The cell-cycle structure enables incorporation of experimental data on cell-cycle phase distribution in different BM compartments as well as radioactive labelling experiments. Moreover, introduction of cell-cycle structure provides a basis for deliberate analysis of chemotherapy-induced toxicity to granulopoiesis, as many of these drugs are cell-cycle phase specific.

The constructed model is employed for evaluating physiological parameters of granulopoiesis dynamics, by a curve-fitting process based on a variety of in vivo experiments. Subsequently, these parameters values are implemented in the mathematical model to enable its validation and comparison to real life results. Having been validated the model is currently used for suggesting minimally toxic schedules of chemotherapeutic drugs monotherapy and optimal combination of these drugs with G-CSF.

2. Methods

2.1. Modelling granulopoiesis

The model of granulopoiesis is formulated as a system of differential equations describing cell numbers and

protein concentrations (G-CSF and G-CSF receptors). The cell equations include terms of proliferation and loss (including cell-cycle structure) and transition between differentiation compartments. Tables 2 and 3 (Appendix C) summarize notations and description of model variables and parameters, respectively.

Previously published models of granulopoiesis considered net proliferation rate, which can change instantaneously according to hormone concentration and cellularity. In contrast, in our physiologically-based approach we model the mitotic compartment by considering the cell-cycle phases, and assuming that the hormonal and micro-environmental feedbacks control the commitment of cells in G_1-phase to proceed to S-phase. Doing so, we aim at increasing the realism of the model and at its consequent validation by retrieving experiments where phase-specific labelling or chemotherapy were applied.

Lacking empirical data on feedback control mechanisms of mitotic cells differentiation we made a reasonable assumption that the transition rates in the first two mitotic sub-compartments are not affected by G-CSF and that the transition rate of the third mitotic sub-compartment depends both on its cellularity and on the concentration of G-CSF (see Section 2.1.2).

The validity of these assumption is supported by experimental BM and blood data (Chatta et al., 1994; Price et al., 1996).

2.1.1. Modelling granulopoiesis in BM

Due to the shortage of reliable quantitative data on dynamics of the earlier progenitor cells in human, and since our preliminary work suggests that such assumption does not compromise the precision of the model's predictions, we simplify stem cell and progenitor dynamics and represent them by a constant inflow of precursors into the myeloblast sub-compartment. This assumption is especially plausible in view of recent experimental data, which show no effect of prolonged G-CSF administration on stem and progenitor cells dynamics in primates (Kuramoto et al., 2004). In our model the number of cells of granulopoietic lineage in the BM is taken as a function of proliferation, transition between compartments and apoptosis rates. We introduce the effect of G-CSF on these three processes as follows: It is assumed that G-CSF activates, through G-CSF receptors, certain intracellular secondary messengers. We assume the existence of three such protein messengers, denoted as x_a, x_1 and x_2. x_a mediates the effect of G-CSF on the probability of mitotic cells to undergo replication, while x_1 and x_2 mediate the effect of G-CSF on the rate of maturation of post-mitotic cells (see Sections 2.1.1, 3.1.2 and 3.1.3). These proteins are stimulated by the level $G(t)$ of G-CSF (at time t). We chose Hill equation as a general form of the dose-effect curves for G-CSF and second messengers influence on maturation and proliferation.

Suppose that the clearance rates of x_a and x_1 are α_a and α_1, respectively. Then an ODE description for the level $x_a(t)$ and $x_1(t)$ of proteins x_a and x_1 is

$$\frac{\mathrm{d}x_i(t)}{\mathrm{d}t} = \lambda_i \frac{G(t)^{u_i}}{G(t)^{u_i} + G_i^{u_i}} - \alpha_i x_i(t), \quad i = a, 1. \tag{1}$$

x_2 is regulated indirectly by G-CSF through the level of x_1. Suppose that the clearance rate of x_2 is α_2. Then an ODE description for the level $x_2(t)$ of x_2 is

$$\frac{\mathrm{d}x_2(t)}{\mathrm{d}t} = \lambda_2 \frac{x_1(t)^{u_2}}{x_1(t)^{u_2} + X_p^{u_2}} - \alpha_2 x_2(t). \tag{2}$$

2.1.2. Transition between compartments

To describe cellular differentiation and maturation we assume that individual cell transition from one compartment to the next occurs after undergoing sufficiently many differentiation and maturation events, which occur with frequency w.

If the waiting time between two consecutive events is exponentially distributed, then the probability of a cell to transit to the next compartment before age τ spent in the current compartment, is given by the Gamma density function (See MacDonald, 1989):

$$\Gamma(\tau, w, n) = \frac{(w\tau)^n \mathrm{e}^{-w\tau}}{n!}\, w, \tag{3}$$

where $n+1$ is the number of maturation events needed for transition and w is their average frequency.

Note that the expected value of this distribution equals $\frac{n+1}{w}$ and the variance is $\frac{n+1}{w^2}$. This enables nearly synchronized migration to blood at a certain age, say $\tau_0(>0)$, by fixing $\frac{n+1}{w} = \tau_0$ and setting a large n (and hence also w) such that the variance is sufficiently small. Alternatively, simple fractional transition can be obtained by setting $n = 0$.

In the above description, the Gamma function distribution covers a wide range of possible maturation dynamics. Its additional advantage lies in the natural and simple way to introduce G-CSF effect on maturation through acceleration of w (see below).

We divide the mitotic compartment into 3 sub-compartments M_i, $i = 1, 2, 3$.

The mitotic sub-compartments M_1 and M_2 are characterized by a time-independent transit flow

$$C_i(\tau) = \Gamma(\tau, w_i, n_i), \quad i = 1, 2. \tag{4}$$

The distribution functions which correspond to the density functions above are given by

$$\varphi_i(\tau) = \int_{\theta=0}^{\tau} C_i(\theta)\,\mathrm{d}\theta = 1 - \sum_{j=0}^{n_i} \frac{(w_i\tau)^j \mathrm{e}^{-w_i\tau}}{j!}, \quad i = 1, 2. \tag{5}$$

These are the probabilities to undergo $n+1$ maturation events (and hence migrate to the next compartment) by the age of τ.

In the case of the M_3 mitotic sub-compartment and the PMC, we represent the effect of G-CSF (whose level at time t is $G(t)$) on the transition rates $C_i(\tau,t)$ as increasing the frequency of maturation events, w, as follows

$$C_i(\tau,t)=\Gamma(\tau,w_i(t),n_i),\quad i=3,4. \tag{6}$$

The frequency $w_3(t)$ in M_3 mitotic sub-compartment is given by

$$w_3(t)=\max\{w_3^s,\tilde{w}_3(t)\}, \tag{7}$$

$$\tilde{w}_3(t)=\lambda_w\left(1+\frac{N_p}{N_3(t)}\,(b+\mathrm{e}^{\frac{-G(t)}{c}})\right)^{-n_w}+W_3^*,\quad n_w,\lambda_w,b,c>0, \tag{8}$$

where $N_3(t)$ is the total number of myelocytes at time t and w_3^s is a steady state value of w_3.

Eq. (7) guarantees that $w_3(t)$ does not decrease below the steady state value. In Eq. (8), $\tilde{w}_3(t)$ is an increasing function of myelocytes cellularity level.

Being the main driving force for mature neutrophil production in response to G-CSF stimulation, Eq. (8) guarantees that myelocytes are being transferred to the PMC faster when they are in abundance. This constraint is important as it prevents excess of BM myelocytes following repeated high doses G-CSF administrations, thus enabling adequate response to each administration (Chatta et al., 1994).

Eq. (8) introduces the direct effect of G-CSF on $w_3(t)$. This effect results in an immediate flow of myelocytes into the PMC in response to a sharp increase in blood G-CSF concentration. Such an immediate reaction should compensate for PMC depletion, which may be caused by massive G-CSF-induced migration of post-mitotic cells into blood, given the time-delay of the effect of increased proliferation in mitotic compartment (due to cell cycle duration).

Maturation frequency in the PMC is expressed as a sum of the effects of short-lived and long-lived intracellular messengers, $x_1(t)$ and $x_2(t)$, respectively:

$$w_4(t)=\mu_1\frac{x_1(t)^{m_1}}{x_1(t)^{m_1}+X_1^{m_1}}+\mu_2\frac{x_2(t)^{m_2}}{x_2(t)^{m_2}+X_2^{m_2}}+W_4^*,\quad m_1,m_2>0. \tag{9}$$

2.1.3. Proliferation and cell-cycle

We unify the cell-cycle phases G_0 and G_1 and further denote them G_1. The rate of entrance of cells in the mitotic sub-compartments into the S-phase (denoted by $A_i(t)$, $i=1,2,3$) is assumed to be age-independent. It does depend on the level $G(t)$ of G-CSF, through $x_a(t)$:

$$A_i(t)=\beta_i\frac{x_a(t)^{l_i}}{x_a(t)^{l_i}+X_a^{l_i}}+A_i^*,\quad l_i>0,\ \ i=1,2,3. \tag{10}$$

Here $\beta_i+A_i^*$ is the maximal rate of transition into the S-phase in compartment i. Ages are reset to zero upon compartment transition. Only cells in G_1 phase can transit to the next compartment.

2.1.4. Apoptosis

There is no agreement in literature about the magnitude of apoptosis in PMC in the normal BM (Mary, 1984). Quantitative in vivo information on apoptosis during G-CSF administration is also lacking, even though the anti-apoptotic effect of G-CSF on neutrophils is well known in vitro (Cowling and Dexter, 1994). Therefore, we assume that cells in the PMC can undergo apoptosis and evaluate its magnitude using data on neutrophil dynamics during G-CSF administration. Apoptosis rate in the PMC decreases exponentially with increase in G-CSF, and also depends on the post-mitotic cellularity when it rises above the normal steady-state value (N_4^s).

$$h(t)=H\frac{\mathrm{e}^{-\eta G(t)}}{d+\left(\frac{N_4^s}{\max\{N_4^s,N_4(t)\}}\right)^{n_h}}. \tag{11}$$

2.1.5. Age equations

The amounts of cells in each compartment i at time t, $N_i(t)$ are given by the age functions $\psi_i(\tau,t)$, such that $N_i(t)=\int_{\tau=0}^{\infty}\psi_i(\tau,t)\,\mathrm{d}\tau$, where the subscripts $i=1,2,3$ correspond to the mitotic sub-compartments and $i=4$ to the PMC. With the above notation, we formulate the following differential equations for the age functions $\psi_i(\tau,t)$.

2.1.5.1. Mitotic compartment. We put forward time-delay equations for the different cell-cycle phases of the mitotic sub-compartments, under the aforementioned assumptions. The total duration of phases S, G_2 and M is taken as a constant T_c.

Let $\psi_{r_i}(\tau,t),\psi_{c_i}(\tau,t)$ denote the numbers of resting (G_0 and G_1) and cycling (S, G_2 and M) cells, respectively, of age τ at time t in the ith mitotic sub-compartment ($i=1,2,3$).

$$\psi_i(\tau,t)=\psi_{r_i}(\tau,t)+\psi_{c_i}(\tau,t). \tag{12}$$

Note that the age functions $\psi_i(-,-)$ are non-zero only when their first component (corresponding to the age) is nonnegative. The equation for resting cells is

$$\frac{\partial\psi_{r_i}(\tau,t)}{\partial\tau}+\frac{\partial\psi_{r_i}(\tau,t)}{\partial t}=\left[-A_i(t)-\frac{C_i(\tau)}{1-\varphi_i(\tau)}\right]\psi_{r_i}(\tau,t)+Inf_i^{M\to G_1}(\tau,t). \tag{13}$$

The transition rate term $\left(\frac{C_i(\tau)}{1-\varphi_i(\tau)}\right)$ is designed so that in the absence of any other effect (proliferation, apoptosis,

etc.) the solution of the equation is

$$\psi_i^s(\tau) = inf_{\to i}^s[1 - \varphi_i^s(\tau)]. \quad (14)$$

The term $A_i(t)$ is the outflow from the G_1 phase into the S phase and $Inf_i^{M\to G_1}(\tau, t)$ is the inflow from the M-phase to G_1, which equals twice the inflow from G_1 to S-phase at $t - T_c$

$$Inf_i^{M\to G_1}(\tau, t) = 2A_i(t - T_c)\psi_{r_i}(\tau - T_c, t - T_c). \quad (15)$$

As mentioned above, cells of age 0 are those who entered the next compartment, therefore following boundary condition is applied

$$\psi_{r_i}(0, t) = \int_{\tau=0}^{\infty} \frac{C_{i-1}(\tau)}{1 - \varphi_{i-1}(\tau)} \psi_{r_{i-1}}(\tau, t)\,\mathrm{d}\tau, \quad i = 2, 3 \quad (16)$$

and

$$\psi_{r_1}(0, t) = Inf_{ST}. \quad (17)$$

The term Inf_{ST} is the inflow of progenitors into the first mitotic sub-compartment. It is assumed to be constant and independent of G-CSF concentration.

An expression for cycling cells reflects the inflow from G_1 during the past T_c time units:

$$\psi_{c_i}(\tau, t) = \int_{\theta=t-T_c}^{t} A_i(\theta)\psi_{r_i}(\tau - t + \theta, \theta)\,\mathrm{d}\theta, \quad (18)$$

where index θ runs over the time of entrance to the S phase.

2.1.5.2. Post-mitotic compartment (PMC). The terms of the PMC equation are cell loss due to apoptosis and transition to the blood

$$\frac{\partial\psi_4(\tau, t)}{\partial\tau} + \frac{\partial\psi_4(\tau, t)}{\partial t} = \left[-h(t) - \frac{C_4(\tau, t)}{1 - \varphi_4(\tau, t)}\right]\psi_4(\tau, t). \quad (19)$$

The boundary condition $\psi_4(0, t)$ corresponds to the total amount of cells transiting from the third mitotic sub-compartment:

$$\psi_4(0, t) = \int_{\tau=0}^{\infty} \frac{C_3(\tau)}{1 - \varphi_3(\tau)} \psi_{r_3}(\tau, t)\,\mathrm{d}\tau. \quad (20)$$

2.1.6. G-CSF dynamics

Based on animal data (Liu and Tang, 1997), we assume that G-CSF concentration $G(t)$ is the same in the blood and in the BM. G-CSF interaction with its receptor is essentially described by the chemical association-dissociation reaction

$$G + r \leftrightarrow q \to internalization, \quad (21)$$

where r, q denote the amounts of the free and bound G-CSF receptors, respectively. Kuwabara et al. (1996b) estimated experimentally that rate of bound receptor internalization is at least an order of magnitude higher than the rate of receptor-ligand dissociation. This enabled us to neglect the receptor-ligand dissociation process and assume that each of the G-CSF–G-CSF receptor complexes is irreversibly destined for internalization. Consequently, the relevant chemical reaction is reduced to

$$G + r \to q. \quad (22)$$

Therefore, receptors dynamics can be described using their age distribution as follows:

$$r(t) = r_b(t) + \sum_{i=1,2,3,4} \int_{\tau=0}^{\infty} r_i(\tau, t)\,\mathrm{d}\tau, \quad (23)$$

where $r_i(\tau, t)$ is the amount of free receptors on cells of age τ in compartment i and $r_b(t)$ is the amount of free receptors in the blood, all given at time t.

In addition to the association–dissociation process, we assume constant production of free receptors in each compartment. Equations for free receptors in each BM compartment are:

$$\begin{aligned}\frac{\mathrm{d}r_b(t)}{\mathrm{d}t} &= -k_1 r_b(t)G(t) - \alpha_b r_b(t) + vN_b(t) \\ &\quad + \int_{\tau=0}^{\infty} \frac{C_4(\tau, t)}{1 - \varphi_4(\tau, t)} r_4(\tau, t)\,\mathrm{d}\tau,\end{aligned}$$

$$\begin{aligned}\frac{\partial r_4(\tau, t)}{\partial\tau} + \frac{\partial r_4(\tau, t)}{\partial t} &= -k_1 r_4(\tau, t)G(t) - \frac{C_4(\tau, t)}{1 - \varphi_4(\tau, t)} r_4(\tau, t) \\ &\quad + v\psi_4(\tau, t) - h(t)r_4(\tau, t),\end{aligned}$$

$$\begin{aligned}&\frac{\partial r_i(\tau, t)}{\partial\tau} + \frac{\partial r_i(\tau, t)}{\partial t} \\ &= -k_1 r_i(\tau, t)G(t) - \frac{C_i(\tau)\psi_{r_i}(\tau, t)}{(1 - \varphi_i(\tau))\,\psi_i(\tau, t)} \\ &\quad \times r_i(\tau, t) + v\psi_i(\tau, t), \quad i = 1, 2, 3.\end{aligned} \quad (24)$$

Initial conditions (receptors amount at age $\tau = 0$) for the BM compartments are:

$$\begin{aligned}&r_i(0, t) = \int_{\tau=0}^{\infty} \frac{C_{i-1}(\tau)\psi_{r_{i-1}}(\tau, t)}{(1 - \varphi_{i-1}(\tau))\psi_{i-1}(\tau, t)} r_{i-1}(\tau, t)\,\mathrm{d}\tau, \\ &\quad i = 2, 3, 4, \\ &r_1(0, t) = 0.\end{aligned} \quad (25)$$

The equation for G-CSF concentration is

$$\frac{\mathrm{d}G(t)}{\mathrm{d}t} = Prod + Adm(t) - k_1 r(t)G(t) - \alpha_G G(t), \quad (26)$$

where

- k_1 is receptor association rate.
- $Prod$ and $Adm(t)$ are the internal production and the administered G-CSF respectively. We assume that the internal G-CSF production is constant. α_G is the non-specific elimination rate of G-CSF by the kidneys (see below).
- $N_b(t)$ is the total number of cells in blood.
- v is the rate of production of free receptors by a cell, which is also assumed to be constant.

We have estimated the non-specific clearance rate α_G using clinical results (Shimazaki et al., 1995) where G-CSF was administered subcutaneously (at time $t = 0$) to patients who had undergone a massive chemotherapy treatment. At that stage both blood and BM were depleted of neutrophils and, hence, it is assumed that no specific clearance of G-CSF occurs. Eq. (26) reduces to the equation:

$$\frac{dG(t)}{dt} = Prod + Adm(t) - \alpha_G G(t). \tag{27}$$

We assume first order absorption from the injection site with absorption rate α_{abs}. Denoting the ratio of injected dose to the volume of distribution by Z_0, we obtain an expression for $Adm(t)$ (which is in fact the inflow of exogenous G-CSF to the blood)

$$Adm(t) = \alpha_{abs} Z_0 e^{-\alpha_{abs} t}. \tag{28}$$

A solution to Eq. (27) is given by

$$G(t) = \frac{Prod}{\alpha_G} + \frac{\alpha_{abs} Z_0}{\alpha_G - \alpha_{abs}} e^{-\alpha_{abs} t} + \left(G(0) - \frac{Prod}{\alpha_G} - \frac{\alpha_{abs} Z_0}{\alpha_G - \alpha_{abs}} \right) e^{-\alpha_G t}. \tag{29}$$

2.1.7. Modelling granulopoiesis in blood

The neutrophil number in the blood is represented by the ODE:

$$\frac{dN_b}{dt} = -\alpha_b N_b + Inf_{\to b}(t), \tag{30}$$

where α_b is fractional loss of blood neutrophils (Dancey et al., 1976), and inflow into the blood $Inf_{\to b}(t)$ from the PMC is

$$Inf_{\to b}(t) = \int_{\tau=0}^{\infty} \frac{C_4(\tau, t)}{1 - \varphi_4(\tau, t)} \psi_4(\tau, t)\, d\tau. \tag{31}$$

We adopt experimental results, which demonstrate that G-CSF does not affect neutrophil dynamics in blood (Price et al., 1996).

2.2. Model validation procedure

The system of equations (1,2,7–11,13,15,16,19, 24–26,30) and (31) constitute the model of human granulopoiesis, which was further analysed in this work. This system was not amenable either to analytic solution or to rigorous steady state analysis. Consequently, the analysis was restricted to numerical simulations of system behavior under a range of biologically plausible values of the parameters. To validate the prediction accuracy of the described mathematical model it was first required to evaluate the model's parameters in humans, by a "curve fitting" process. In case of adjustment of up to 4 parameters in an explicitly formulated equation, we used the Marquardt—Levenberg algorithm for fitting model computation output to the respective clinical results taken from the literature. In case of a system of several analytically unresolvable differential equations, they were transformed into difference equations and the behavior of the system was simulated using a computer program written in C++ under Visual studio. NET environment.

It can be easily seen that the positivity of the solution of all differential equations in the model for all t is guaranteed if the initial values of the model state variables are not negative, and $A_i(t)$ and $w_i(t)$ are positive for all t. During parameter evaluation procedure positivity of these functions was imposed. The biological and pharmacokinetics (PK)/pharmacodynamics (PD) parameters were iteratively adjusted within the range of potential real-life values, so as to most accurately retrieve the experimental results. To this end we used the granulopoiesis simulation model described above, empirical data (see Results section for details), and an efficient search algorithm (e.g. modified Powell's conjugate directions method, Brent, 1973; Press et al., 1993). Once human granulopoiesis parameters were evaluated, they were implemented in the model and its predictions were compared with experimental results. Additionally, to check a general behavior of the system we have run simulations of the resultant model under wide range of physiologically relevant initial conditions and external perturbations including administration of different doses of G-CSF and elimination of different fractions of BM cells (data not shown). $A_i(t)$ and $w_i(t)$ did not approach zero values during these simulations. Moreover, in case of the application of initial values of the variables within the normal physiological ranges (Table 2, see Appendix C) under the aforementioned set of parameters (Table 3, see Appendix C), the system returned to its initial state after all perturbations examined.

3. Results

3.1. Parameter evaluation

Granulopoiesis parameters that are essential to the model, were evaluated by fitting the simulation results to clinical data, as follows: Absorption of G-CSF and its non-specific clearance rates were evaluated from experimental data of G-CSF PK in severely neutropenic patients; steady-state compartment sizes and transition functions in post-mitotic and M_3 compartments, as well as steady-state proliferation fraction in M_3 were evaluated from radioactive labelling experiments in patients with intact granulopoiesis; parameters of G-CSF PD in the post-mitotic compartment were evaluated from blood neutrophil counts and G-CSF concentrations in healthy volunteers following a single

G-CSF administration; other parameters of G-CSF PD and parameters of G-CSF specific clearance were evaluated from blood neutrophils and BM data in healthy volunteers following multiple G-CSF administrations. Evaluated parameters are summarized in Table 3, which also presents published data for parameters and steady state variable values, previously evaluated experimentally. The precision of these estimations was manifested while using the model to retrieve experimental data, as described hereafter.

3.1.1. Absorption and non-specific clearance rate of G-CSF

In Fig. 1 we show the curve fitting of our model to clinical results in Shimazaki et al. (1995), where G-CSF concentration in blood was followed in severely neutropenic patients after a single subcutaneous injection of G-CSF. The values of α_{abs} and α_G, which were obtained by fine-tuning the model parameters to results of the clinical experiment are presented in Table 3. These parameters were used in further parameter evaluation (see below).

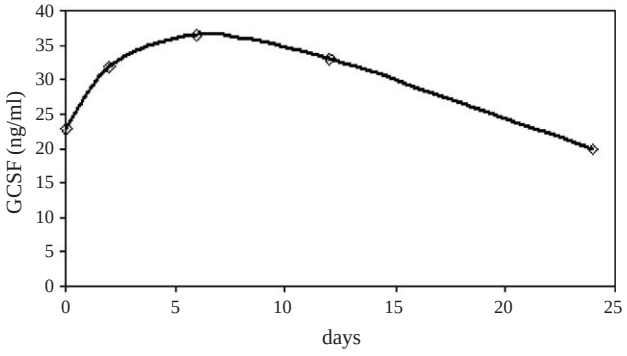

Fig. 1. Model retrieval of G-CSF concentration in blood (in ng/ml) following a single subcutaneous injection to two severely neutropenic patients. Non-specific clearance and absorption rates of G-CSF were evaluated; circles—experimental data from Shimazaki et al. (1995), line—best fit of the mathematical model using Eq. (29). Evaluated parameters are listed in Table 3.

3.1.2. Myelocytes (M_3) and postmitotic compartments in steady-state

In (Fig. 2) Steinbach et al. (1979), mitotic cells were continuously labelled (from time $t = 0$, say) with H^3—*thymidine* in two brain cancer patients (no involvement of BM by the disease), and the appearance of labelled PMNs in the peripheral blood was followed between $t = 100$ h and $t = 300$ h following the injection. We fitted our model parameters to these experimental curves. Our results show that Gamma distribution of maturation events can fit the experimental data with high precision and that the dynamics of radioactivity in the blood of these patients depends solely on 3 parameters (see below and Appendix B). The radioactivity index is given in Steinbach et al. (1979) as percentage of the maximal index. We assume that from time $t = 0$ all cells entering the PMC are labelled.

We fitted the curves in Steinbach et al. (1979) with Eq. (B.9) (see also methods section). Note that the parameters w_4^s, h^s, representing the frequency of maturation events in the PMC and the apoptosis rate (both at a steady-state), cannot be resolved separately. Note also that the value of α_b was taken from Dancey et al. (1976). We calculated average transit-time in the post-mitotic compartments according to Eq. (A.13) to be 124 and 131 h for each patient respectively.

In addition, we used another independent experiment (Cartwright et al., 1964) in conjunction with data on cellularity levels of the different BM compartments (Dancey et al., 1976), for evaluating the transit-time of the myelocytic compartment and the total number of cells in the myelocyte, post-mitotic and blood compartments, and for testing the generality of our previous evaluation of post-mitotic parameters. In this experiment healthy volunteers were injected by DFP^{32}, for

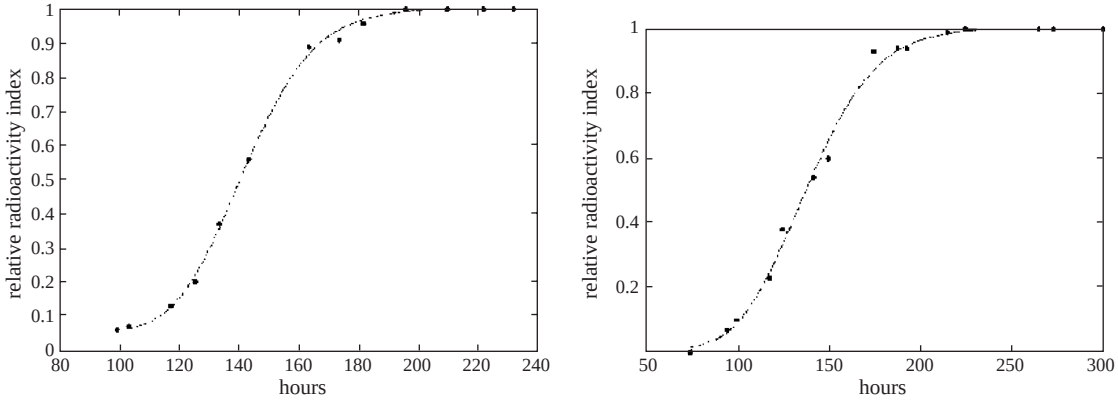

Fig. 2. Simulation of continuous labelling of granulocytes with H^3—*thymidine*. Circles represent experimental data from Steinbach et al. (1979): two brain cancer patients received continuous intravenous infusion of radioactive thymidine from time $t = 0$, followed by repetitive measurements of PMN-associated radioactivity in blood in relative units. The broken line represents the fit of the model using Eq. (B.9). x-axis is in hours, y-axis—PMN-associated blood radioactivity index relative to maximal.

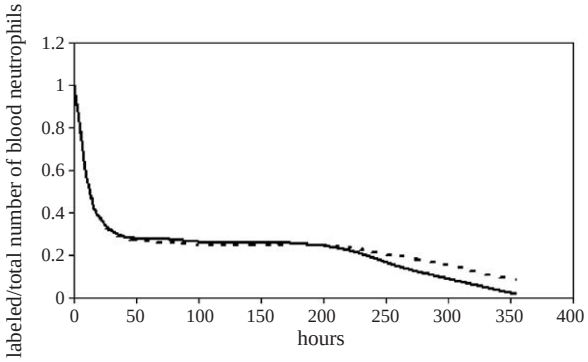

Fig. 3. Simulation of granulocytes pulse labelling with DFP^{32}. Experimental data of granulocytes pulse labelling in human healthy volunteers were taken from Cartwright et al. (1964) (—). The pulse was applied at time $t = 0$. Ratio of labelled to non-labelled blood neutrophils over time is presented. Model parameters of post-mitotic and myelocyte compartments were evaluated by best fit to the data (- - -) (see text).

labelling blood neutrophils, post-mitotic cells and myelocytic cells. The ratio of labelled to total blood neutrophils had been monitored over time (Fig. 3). We then evaluated the model parameters sequentially according to Cartwright et al. (1964). The resultant best fit curve is displayed in Fig. 3.

The first rapid descent of the curve in Fig. 3 corresponds to the disappearance of labelled blood neutrophils, whose labelling intensity is 4 times higher than in BM. PMN turnover rate in blood was taken from Dancey et al. (1976), and it resulted in a very good fit. The best fit of the plateau and second descent parts of the curve was achieved with post-mitotic transit-time of 180 h, which is significantly longer than 130 h estimate obtained from fitting Steinbach et al. (1979). Unable to resolve this discrepancy, we assumed an intermediate value of 168 h (7 days) as the post-mitotic time in further parameter evaluation, which is very close to 6.6 days estimation in Dancey et al. (1976). We also estimated the fraction of cells undergoing apoptosis in the post-mitotic compartment at steady-state. This fraction was calculated as unity minus ratio between outflow and inflow in PMC (see Section A.1 Eq. (A.7)). The resultant value was 57%.

3.1.3. Granulopoiesis parameters under G-CSF administration

3.1.3.1. Granulopoiesis under single G-CSF administration. In this section, we reproduced clinical results reported in de Haas et al. (1994), where four healthy volunteers received subcutaneously a single dose of 300 μg G-CSF; PMN cells and G-CSF concentration in peripheral blood were followed for 4 days post injection. Price et al. (1996) demonstrated that after prolonged administration of such a G-CSF dose, cells labelled in the mitotic compartment enter blood after 48 hours, or more. Thus, we assumed a constant (or zero) inflow from M_3 into the post-mitotic compartment during this period. This assumption enabled to restrict the searched parameters to those of PMC only. The experimental results were simulated using Eqs. (9), (11), (19), (30), (31), with normal steady-state cell distribution derived in Section 3.1.2 as an initial condition. In this simulation we used experimentally measured concentrations of G-CSF, as reported in the original article (de Haas et al., 1994).

When comparing the simulation results of the present experiment with G-CSF and blood neutrophil data in de Haas et al. (1994), one notes an 8 h delay between the peaks of blood neutrophils and G-CSF concentration. Moreover, a delay of 3 days can be observed between baseline recovery timings of neutrophils and G-CSF. Consequently, it is not surprising that experimental curve could not be retrieved when G-CSF effect on $w_4(t)$ was initially modelled as direct function of blood G-CSF concentration (Fig. 4). This result led us to conclude that G-CSF has a significant cumulative effect on the post-mitotic compartment. Making this assumption, the half-life of x_1 was set within the experimental half-life range of STATs (Siewert et al., 1999), while longer half-life of x_2 corresponds to induction of late proteins downstream to activated STATs. Data in de Haas et al. (1994) were best fitted when clearance rate of long-living messenger (α_2) was very slow (0.008 hour) (Fig. 4).

3.1.3.2. Granulopoiesis under multiple G-CSF administration. In order to test generality of the granulocyte dynamic parameters, which were assessed using clinical results of a single G-CSF dosing, we also applied our model to experimental data of multiple G-CSF administrations, provided by Chatta et al. (1994). In this trial rhG-CSF was administered daily to healthy young and elderly volunteers during 14 days. Two doses (30 or 300 μg per day) of rhG-CSF were given to randomized groups of volunteers and their blood neutrophils were

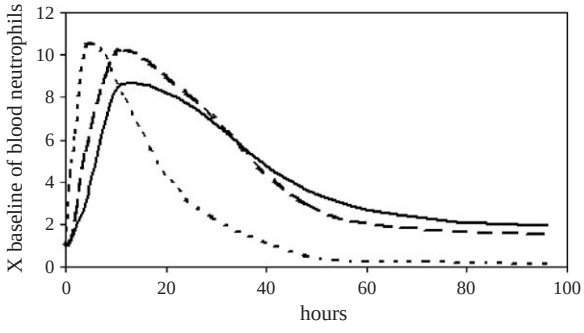

Fig. 4. Simulation of blood neutrophil dynamics following a single dosing of G-CSF. A dose of 300 μg of rhG-CSF was administered subcutaneously to healthy volunteers (de Haas et al., 1994), followed by sequential measurements of blood PMN counts (—). Parameters of the post-mitotic compartment were evaluated both when the granulopoiesis model assumed (- - -) or ignored (. . .) the cumulative effect of G-CSF by intracellular second messenger (see text).

counted during 15 days. Parameters of G-CSF and G-CSF receptor dynamics were taken from the literature (see Table 3), with the exception of absorption rate from the injection site and non-specific clearance, which were retrieved separately (Section 3.1.1). Mean post-mitotic transit-time was allowed to fluctuate between steady-state value of 7 days (3.1.2) and minimal value of 2 days (as evaluated in Price et al. (1996)).

Results show that when the post-mitotic compartment parameters, derived in Section 3.1.3, are employed in the multiple dosage scenario, they fail to reproduce the daily fluctuations in PMN count seen in Chatta et al. (1994) (data not shown). Our results further suggest that this

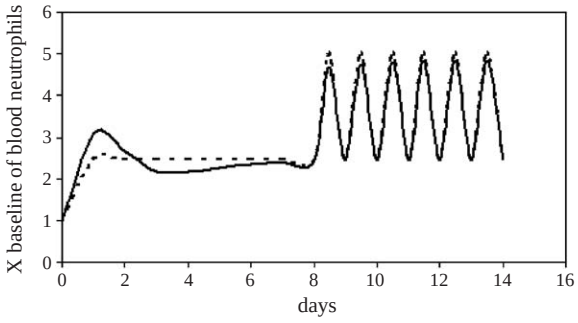

Fig. 5. Simulation of blood neutrophil dynamics following multiple rhG-CSF dosings. Thirty microgram per day of rhG-CSF was administered subcutaneously to healthy volunteers (Chatta et al., 1994), followed by sequential measurements of blood PMN counts every 24 h for the first 8d, and every 12 h for additional 7d (—). Model parameters were evaluated by fit to this curve only (- - -).

effect stems from α_2 being relatively low in the single-dose case and relatively high in multiple dose case. This corresponds to prolonged half-life of the second messenger in the single dose case, as compared to the multiple-dose case, where there is relatively rapid decrease of neutrophil counts after the peak. Therefore, we now performed a new, independent, evaluation of all the parameters, including α_2 for the multiple dose scenario. Data in Chatta et al. (1994) were best fitted by our model when α_2 was very fast (0.2 h) (see Fig. 5). The meaning of this result is that the assumption of prolonged half-life of the second messenger is essential for reproducing a single G-CSF regimen, while short half-life is necessary in case of multiple administrations. However, in order not to make the model unnecessarily complex, we used an intermediate value of α_2 in order to retrieve further results of single, as well as multiple, treatment schedules. The results shown in Fig. 6 suggest that this intermediate value still enables curve fitting of appreciably high precision of both single and multiple administrations of G-CSF.

3.2. Validation of model predictions

The model's predictions were validated by their comparison to new sets of published experimental data. The first validation experiment involved the volunteers described in Chatta et al. (1994). These subjects had undergone BM biopsies at days 0 and 7 of G-CSF administration, as well as pulse labelling of proliferative

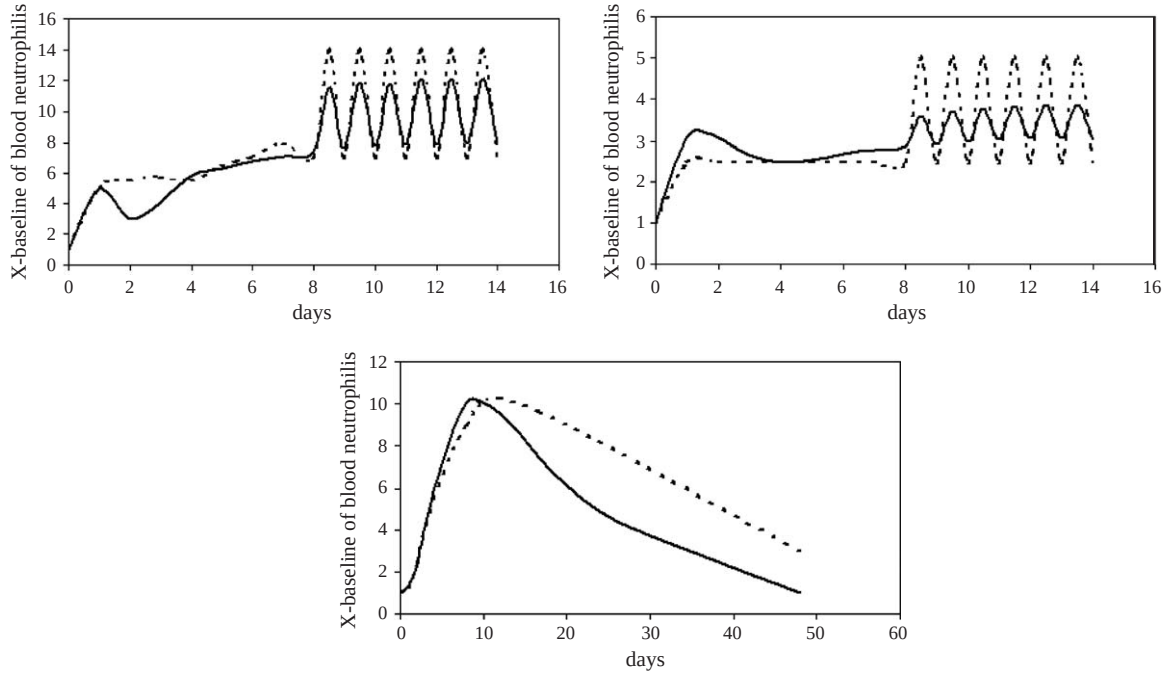

Fig. 6. Simultaneous simulation of multiple and single G-CSF administration. Upper panel: multiple G-CSF administration. See Fig. 5 for details; left: 300 μg/d. right: 30 μg/d. Lower panel: single G-CSF administration. See Fig. 4 for details. Parameters were evaluated simultaneously for all three data sets. Experimental data (—). Model prediction (- - -).

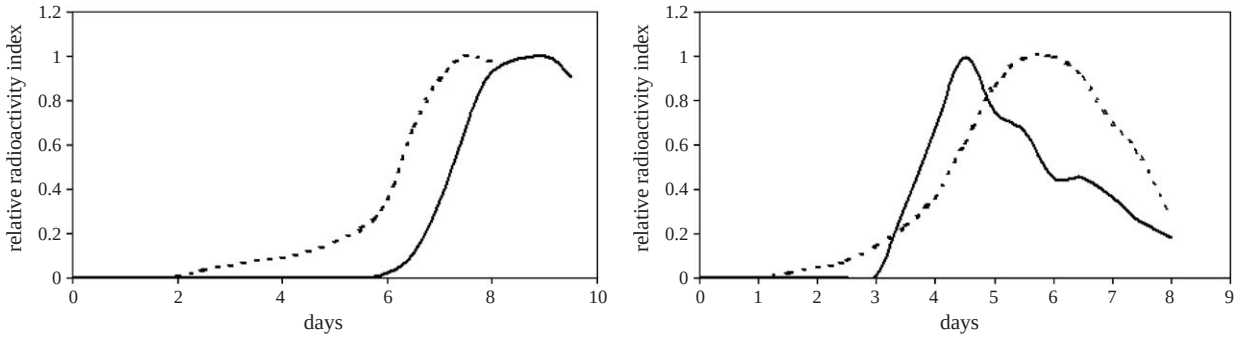

Fig. 7. Simulation of pulse labelling of granulocytes by H^3—*thymidine*. Healthy volunteers were injected by H^3—*thymidine* before, as well as 5d following, the onset of daily administration of 30 μg/d G-CSF. Index of PMN-associated radioactivity in blood was subsequently measured for several days (Price et al., 1996) (—). Model prediction (- - -) is presented versus real-life measurements. G-CSF left: day 0. right: day 5.

Table 1
Simulation of BM granulocyte counts following G-CSF administration

Compartment	Experimental data	Simulation
Myeloblasts	1	1
Pro-myelocytes	3.5	3
Myelocytes	2.7	1.7
Post-mitotic	1.3	1.3

Volunteers described in Chatta et al. (1994) underwent BM biopsies at days 0 and 7 following administration of 300 μg/d G-CSF. Model predictions can be compared to experimental measurements of total cellularity in each of the marrow compartments relative to the steady-state level.

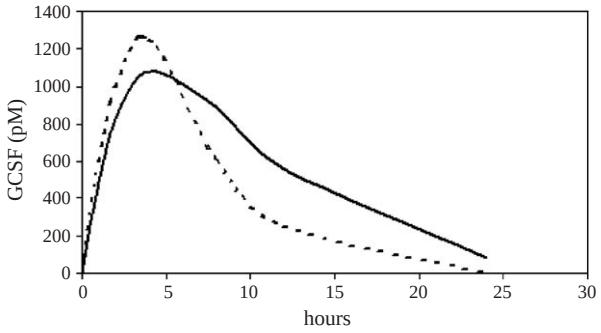

Fig. 8. Simulation of G-CSF PK. Blood G-CSF concentrations were experimentally measured following subcutaneous administration of single 300 μg G-CSF dosing (de Haas et al., 1994) (—). Model predictions (- - -) can be compared with experiment.

granulocytes with H^3—*thymidine*; radioactive granulocytes were monitored in blood starting on days 0 or 5 (Price et al., 1996). We validated the precision of our model predictions by simulating the above experiment using the parameters evaluated simultaneously by the experimental results in Chatta et al. (1994) and de Haas et al. (1994) and comparing the predictions with experimental results. To this end we introduced in the model H^3—*thymidine* labelling as similar, instantaneous, labelling of all S-phase cells in the BM and reduction of labelling-intensity per cell upon cell division. As can be seen in Fig. 7 and Table 1 predictions of our model are very close to the experimental data. The delayed radioactivity peak at steady-state appearing in Fig. 7 (left) is due to our use of intermediate post-mitotic transit-time estimate (between Price et al. (1996) and Cartwright et al. (1964)). One notices, also, that the radioactivity wave in blood lasts somewhat longer in the experiment than it does in the simulation (Fig. 7 right). This difference is attributable to the re-uptake of H^3—*thymidine* by BM cells (Mary, 1984), which was ignored in the model.

We compared the simulation results of G-CSF concentration following a single G-CSF dosing with the experimental curve in de Haas et al. (1994). The results (see Fig. 8) are in a good agreement with experiment.

In addition, we estimated the mean number of G-CSF receptors per blood neutrophil at steady-state conditions. Our model prediction gave value of 2200, which is also very close to experimental results in human (Shinjo et al., 1995).

4. Discussion

The granulopoiesis model we constructed in this work accurately retrieved various clinical results including radioactive labelling experiments and different G-CSF administration regimens. We show that the experimental curves of G-CSF PD could not be retrieved by the model simulations without assuming a long-lasting cumulative G-CSF effect. This effect was modelled by introducing intracellular second messenger as a mediator of cellular effect of G-CSF. It should be noted that this result is corroborated by experiments: it is well known that G-CSF effect is mediated by STAT family of transcription factors (Siewert et al., 1999; McLemore et al., 2001; Dong et al., 1998). We believe that this cumulative effect of G-CSF had been ignored in previous granulopoiesis models, since it was never

attempted to employ such models for simultaneous reproduction of the experimental PMN counts and G-CSF concentration in blood. Our results suggest prolonged half-life of the second messenger under a single administration of G-SCF and shorter half-life after prolonged G-CSF treatment. This phenomenon can be explained by down-regulation of the second messenger's effect by its accelerated clearance, which is plausible biologically based on the experimental data on down-regulation of STAT proteins by specific intracellular domain of G-CSF receptor (Dong et al., 1998, 2001). Once quantitative data of this down-regulation will be experimentally available, it can be incorporated in the mathematical model.

Several authors attempted to estimate the magnitude of ineffective granulopoiesis (apoptosis) in the post-mitotic compartment by comparing blood neutrophil turnover with BM neutrophil production. This estimation method has led to controversial results (reviewed in Mary, 1984). It appears that the estimation precision of the latter method is compromised by necessity to evaluate several variables, that were not, or cannot be, concurrently measured, such as PMC absolute size, marginal pool of blood neutrophils and PMC transit-time. For example, direct immuno-histological staining of apoptotic cells in the normal BM shows that their incidence is very low (1–5%) (Irvine et al., 1998; Ogawa et al., 2000). However, in order to use this incidence for calculation of ineffective granulopoiesis index (ratio of outflow from PMC into blood to inflow from MC into PMC) one must take into account "transit-time" of apoptotic cell in BM as determined by the elimination efficiency of apoptotic cells by BM macrophages, which currently cannot be assessed experimentally. Another example is the work of Mackey et al. (2003) who evaluated both apoptosis-rate and elimination-rate of apoptotic cells from the post-mitotic compartment using steady-state experimental data in a simple mathematical model. Note, though, that these authors' calculations could be compromised as they used anti-CD15 antibodies for staining post-mitotic compartment, while these antibodies stain also to some degree dividing granulocyte precursors (Iwasaki et al., 1999). Our model of granulopoiesis is new in explicitly including G-CSF-dependence of apoptosis in PMC neutrophil dynamics. Our estimate of net steady-state apoptosis-rate is 57%, based on the use of our model in conjunction with the experimental data in de Haas et al. (1994) and Cartwright et al. (1964). Interestingly, it is very close to the estimate of Mackey et al. (2003) despite the fact that we used completely different type of data and quite different mathematical model.

The good precision of our model predictions, which has been retrospectively validated in this work, is encouraging. At present we use this model for suggesting new regimens of chemotherapeutic and supportive drug therapy that will minimize the risks of neutropenia in oncological patients.

Acknowledgements

The authors wish to thank Y. Kogan and S. Fleishman for fruitful discussion, and the Chai Foundation for financial support.

Appendix A. Steady-state equations

Since the system of equations describing granulopoiesis includes non-linear differential equations with delay (mitotic compartment), formal mathematical analysis of the system (including existence of steady-state and its stability) is extremely difficult. Consequently, we performed the following analysis of granulopoiesis at normal steady-state. Firstly, we assumed a constant G-CSF concentration (set at its normal concentration in human) and calculated relationships between transition and proliferation functions and compartment sizes. These relationships were subsequently used for calculating steady-state parameters, based on the published experimental data on compartments' sizes. Here we describe the relevant equations. Steady-state parameters are denoted by superscript s.

We assume steady-state

$$2Inf_i^{G_1\to S} = Inf_i^{M\to G_1}, \quad i = 1,2,3. \tag{A.1}$$

Since multiplication of cells during mitosis is instantaneous we can write following expression for total amounts of resting and cycling cells in the mitotic sub-compartments

$$N_{c_i}^s/T_c = N_{r_i}^s A_i^s, \quad i = 1,2,3. \tag{A.2}$$

Given experimental values of fraction of G_1 phase cells in mitotic compartments (see Table 1) we can calculate A_i^s.

A.1. Transition and apoptosis in the postmitotic compartment

At steady-state blood Eqs. (30) and (31) yield

$$N_b^s = \frac{Inf_{\to b}^s}{\alpha_b} \tag{A.3}$$

and

$$Inf_{\to b}^s = \int_{\tau=0}^{\infty} \frac{C_4^s(\tau)}{1-\varphi_4^s(\tau)}\,\psi_4^s(\tau)\,d\tau. \tag{A.4}$$

In post-mitotic compartment age distribution at steady-state is the result of solution of the time independent

version of Eq. (19):

$$\psi_4^s(\tau) = inf_{\to 4}^s e^{-h^s\tau}[1-\varphi_4^s(\tau)] = inf_{\to 4}^s e^{-h^s\tau}\sum_{i=0}^{n_4}\frac{(w_4^s\tau)^i e^{-w_4^s\tau}}{i!}, \quad (A.5)$$

where

$$inf_{\to 4}^s = \psi_4^s(0) = \int_{\tau=0}^{\infty}\frac{C_3^s(\tau)}{1-\varphi_3^s(\tau)}\psi_{c_3}^s(\tau)\,d\tau \quad (A.6)$$

is the steady-state inflow to PMC.

Putting together Eqs. (A.4) and (A.5) we obtain

$$\begin{aligned} inf_{\to b}^s &= \int_{\tau=0}^{\infty}\frac{C_4^s(\tau)}{1-\varphi_4^s(\tau)} inf_{\to 4}^s e^{-h^s\tau}[1-\varphi_4^s(\tau)]\,d\tau \\ &= inf_{\to 4}^s w_4^s\int_{\tau=0}^{\infty}\frac{(w_4^s\tau)^{n_4}e^{(-h^s-w_4^s)\tau}}{n_4!}\,d\tau \\ &= inf_{\to 4}^s\left(\frac{w_4^s}{w_4^s+h^s}\right)^{n_4+1}\int_{\tau=0}^{\infty}(w_4^s+h^s) \\ &\quad\times\frac{[(w_4^s+h^s)\tau]^{n_4}e^{(-h^s-w_4^s)\tau}}{n_4!}\,d\tau \\ &= inf_{\to 4}^s\left(\frac{w_4^s}{w_4^s+h^s}\right)^{n_4+1}. \end{aligned} \quad (A.7)$$

We develop Eq. (A.5), and make use of the normal compartment size to explore the virtual parameters of maturation.

For the PMC:

$$\begin{aligned} N_4^s &= \int_{\tau=0}^{\infty}\psi_4^s(\tau)\,d\tau = inf_{\to 4}^s\sum_{j=0}^{n_4}\int_{\tau=0}^{\infty}\frac{(w_4^s\tau)^j e^{(-h^s-w_4^s)\tau}}{j!}\,d\tau \\ &= inf_{\to 4}^s\sum_{j=0}^{n_4}\frac{(w_4^s)^j}{(h^s+w_4^s)^j}\int_{\tau=0}^{\infty}\frac{[(h^s+w_4^s)\tau]^j e^{(-h^s-w_4^s)\tau}}{j!}\,d\tau \\ &= inf_{\to 4}^s\sum_{j=0}^{n_4}\frac{(w_4^s)^j}{(h^s+w_4^s)^{j+1}} \\ &= \frac{1}{h^s}inf_{\to 4}^s\left[1-\left(\frac{w_4^s}{(h^s+w_4^s)}\right)^{n_4+1}\right]. \end{aligned} \quad (A.8)$$

Remark. If no apoptosis exists ($h^s=0$), the above expression is simply

$$N_4^s = inf_{\to 4}^s\frac{n_4+1}{w_4^s}. \quad (A.9)$$

From Eqs. (A.3), (A.7) and (A.8) we get

$$\alpha_b N_b^s = Inf_{\to b}^s = Inf_{\to 4}^s - N_4^s h^s. \quad (A.10)$$

By Eqs. (A.7) and (A.10) we get

$$\left(1+\frac{h^s}{w_4^s}\right)^{n_4+1} = \frac{inf_{\to 4}^s}{inf_{\to b}^s} = 1+\frac{N_4^s h^s}{\alpha_b N_b^s}. \quad (A.11)$$

Let T_4^s be the average steady-state transit-time of the PMC defined as average age of post-mitotic cells that enter the blood. Then it can be calculated in the following manner.

The number of cells at age τ that migrate into the blood from the PMC at steady-state is $\frac{C_4^s(\tau)}{1-\varphi_4^s(\tau)}\psi_4^s(\tau)$. Then by Eq. (A.5) with substitution of $\varphi_4^s(\tau)$ from Eq. (5) we have

$$\begin{aligned} T_4^s &= \frac{\int_{\tau=0}^{\infty}\tau\frac{C_4(\tau)}{1-\varphi_4(\tau)}\psi_4(\tau)\,d\tau}{\int_{\tau=0}^{\infty}\frac{C_4(\tau)}{1-\varphi_4(\tau)}\psi_4(\tau)\,d\tau} = \frac{\int_{\tau=0}^{\infty}\frac{(w\tau)^{n+1}e^{-(h+w)\tau}}{n!}d\tau}{\int_{\tau=0}^{\infty}\frac{(w\tau)^n e^{-(h+w)\tau}}{n!}w\,d\tau} \\ &= \frac{\frac{w^{n+1}(n+1)}{(h+w)^{n+2}}\int_{\tau=0}^{\infty}\frac{[(h+w)\tau]^{n+1}e^{-(h+w)\tau}}{(n+1)!}(h+w)\,d\tau}{\frac{w^{n+1}}{(h+w)^{n+1}}\int_{\tau=0}^{\infty}\frac{[(h+w)\tau]^n e^{-(h+w)\tau}}{n!}(h+w)\,d\tau}. \end{aligned} \quad (A.12)$$

$$T_4^s = \frac{n_4+1}{w_4^s+h^s}. \quad (A.13)$$

Note that for convenience we omit superscript "s" and subscript "4" for w, n and h in the interim equations.

Eqs. (A.11) and (A.13) enable to calculate w_4^s and h^s given n_4, N_4^s, α_b, N_b^s and T_4^s. If h^s is known, we can compute $Inf_{\to 4}^s$ from Eq. (A.10). Calculated values of $Inf_{\to 4}^s$, w_4^s and h^s were used in Sections 3.1.2 and 3.1.3.

Appendix B. Continuous radioactive labelling at steady-state

The radioactivity index $RI(t)$ (t is time from the beginning of experiment) is computed as a convolution between the inflow of labelled cells and their elimination in the blood:

$$RI(t) = \int_{\theta=0}^{t} Inf_{\to b}^l(\theta)e^{-\alpha_b(t-\theta)}\,d\theta. \quad (B.1)$$

The inflow $Inf_{\to b}^l(\theta)$ of labelled cells to the blood at time θ under steady-state conditions is

$$Inf_{\to b}^l(\theta) = \int_{\tau=0}^{\theta}\frac{C_4(\tau)}{1-\varphi_4(\tau)}\psi_4(\tau)\,d\tau. \quad (B.2)$$

The cells in this equation are of post-mitotic age which does not exceed θ; This provides that they entered the PMC not before $t=0$ and are thus labelled.

Substitute (A.5) in (B.2):

$$Inf_{\to b}^l(\theta) = \int_{\tau=0}^{\theta} C_4(\tau)Inf_{\to 4}^s e^{-h\tau}\,d\tau. \quad (B.3)$$

Substitute in (B.1) using (3), (4)

$$RI(t) = \int_{\theta=0}^{t} e^{-\alpha_b(t-\theta)}\times\left(\int_{\tau=0}^{\theta}\frac{(w_4\tau)^{n_4}e^{-(w_4+h)\tau}}{n_4!}w_4 Inf_{\to 4}^s\,d\tau\right)d\theta. \quad (B.4)$$

Solving the inner integral we obtain

$$RI(t) = Inf^{s}_{\to 4} \int_{\theta=0}^{t} \mathrm{e}^{-\alpha_b(t-\theta)} \frac{w_4^{n_4+1}}{(w_4+h)^{n_4+1}} \times \left[1 - \sum_{i=0}^{n_4} \frac{[(w_4+h)\theta]^i}{i!} \mathrm{e}^{-(w_4+h)\theta}\right] \mathrm{d}\theta \quad \text{(B.5)}$$

$$= Inf^{s}_{\to 4} \frac{w_4^{n_4+1}}{(w_4+h)^{n_4+1}} \mathrm{e}^{-\alpha_b t} \left[\frac{\mathrm{e}^{\alpha_b t}-1}{\alpha_b} - \sum_{i=0}^{n_4} \int_{\theta=0}^{t} \frac{[(w_4+h)\theta]^i}{i!} \mathrm{e}^{-(w_4+h-\alpha_b)\theta} \mathrm{d}\theta\right]. \quad \text{(B.6)}$$

Another integration gives

$$RI(t) = Inf^{s}_{\to 4} \frac{w_4^{n_4+1}}{(w_4+h)^{n_4+1}} \left[\frac{1-\mathrm{e}^{-\alpha_b t}}{\alpha_b} - \mathrm{e}^{-\alpha_b t} \sum_{i=0}^{n_4} \frac{(w_4+h)^i}{(w_4+h-\alpha_b)^{i+1}} * \left(1 - \sum_{j=0}^{i} \frac{(w_4+h-\alpha_b)^j t^j \mathrm{e}^{-(w_4+h-\alpha_b)t}}{j!}\right)\right]. \quad \text{(B.7)}$$

Since

$$RI(\infty) = Inf^{s}_{\to 4} \frac{w_4^{n_4+1}}{(w_4+h)^{n_4+1}} \alpha_b^{-1} \quad \text{(B.8)}$$

this equation yields

$$\frac{RI(t)}{RI(\infty)} = 1 - \mathrm{e}^{-\alpha_b t} - \alpha_b \mathrm{e}^{-\alpha_b t} \sum_{i=0}^{n_4} \frac{(w_4^s+h^s)^i}{(w_4^s+h^s-\alpha_b)^{i+1}} \times \left(1 - \sum_{j=0}^{i} \frac{(w_4^s+h^s-\alpha_b)^j t^j \mathrm{e}^{-(w_4^s+h^s-\alpha_b)t}}{j!}\right). \quad \text{(B.9)}$$

Appendix C. Parameters and variables

State variables and parameter values (Tables 2 and 3).

Table 2
State variables

Compartment	Description	Notation	Variable[a] Normal value	Type[a]	[Reference]/ (Equation)
Mitotic	Ratio of G_0+G_1 to total number of M_1 cells		45% (20–45)	Lit	[Dormer et al., 1990]
	Ratio of G_0+G_1 to total number of M_2 cells		45% (20–45)	Lit	[Dormer et al., 1990]
	Ratio of G_0+G_1 to total number of M_3 cells		75% (60–75)	Lit	[Dormer et al., 1990]
	Total number of M_1 cells	N_1	2.3×10^7 cells/kg	Opt	
	Total number of M_2 cells	N_2	3.4×10^8 cells/kg	Lit	[Dancey et al., 1976] [Harrison, 1962]
	Total number of M_3 cells	N_3	3×10^9 cells/kg	Lit	[Dancey et al., 1976] [Harrison, 1962]
	Maturation frequency of M_3	w_3	0.5 steps/h	opt	(6)
	Entry rate into s-phase of M_1	A_1	0.081/h	Calc	(10)

Table 2 (*continued*)

Compartment	Description	Notation	Variable[a] Normal value	Type[a]	[Reference]/ (Equation)
	Entry rate into s-phase of M_2	A_2	0.081/h	Calc	(10)
	Entry rate into s-phase of M_3	A_3	0.022/h	Calc	(10)
Post-mitotic	Total number of cells	N_4	7.5×10^9 cells/kg ($4–10 \times 10^9$)	Lit	[Dancey et al., 1976], [Cartwright et al., 1964], [Liu et al., 1983], (A.10)
	Maturation frequency	w_4	0.566 steps/h	Calc	(6)
	Apoptosis rate	h	0.005/h	Calc	(11)
Blood	Total number of cells	N_b	3×10^8 cells/kg ($2–5 \times 10^8$)	Lit	[Mary, 1984], [Dancey et al., 1976], (A.10)
G-CSF	G-CSF concentration	G	2.5 pM (1.5–2.5)	Lit	[de Haas et al., 1994], (29)

[a]Normal human values used as initial conditions.
[a]Type field describes three possible data sources: (1) Lit—obtained from the literature. (2) Opt—optimized. (3) Calc—calculated.

Table 3
Parameters values

Compartment	Description	Notation	Const. Value (Range)	Type	[Reference]/ (Equation)
Mitotic	Cycling time	T_c	15 h	Lit	[Mary, 1984], (18)
	Parameters for dependence of entry rate into s-phase of mitotic compartments on protein x_a	β_1	2/h	Opt	(10)
		l_1	0.001	Opt	(10)
		β_2	0.8/h	Opt	(10)
		l_2	0.1	Opt	(10)
		β_3	2/h	Opt	(10)
		l_3	1.8	Opt	(10)
		X_a	62.18	Opt	(10)
		A_1^*	−0.92/h	Calc	(10)
		A_2^*	−0.23/h	Calc	(10)
		A_3^*	0.02/*h*	Calc	(10)

Table 3 (*continued*)

Compartment	Description	Notation	Const. Value (Range)	Type	[Reference]/ (Equation)
	Maturationsteps number—M_1	n_1	24 steps	Opt	(4)
	Maturation steps number—M_2	n_2	24 steps	Opt	(4)
	Maturation steps number—M_3	n_3	50 steps	Opt	(6)
	Maturation freq. of M_1	w_1	0.36 steps/h	Opt	(4)
	Maturation freq. of M_2	w_2	0.36 steps/h	Opt	(4)
	Parameters for dependence of x_a on G-CSF conc.	λ_a	7.13/h	Opt	(1)
		u_a	0.79	Opt	(1)
		G_a	1000 pM	Opt	(1)
		α_a	0.1/h	Opt	(1)
	Parameters for dependence of w_3 on G-CSF conc. and cellularity of M_3	λ_w	66.6 steps/h	Opt	(8)
		n_w	0.8	Opt	(8)
		N_p	7.3×10^{10} cells/kg	Opt	(8)
		W_3^*	−1.17 steps/h	Calc	(8)
		b	3.08	Opt	(8)
		c	250 pM	Opt	(8)
Post mitotic	Parameters for dependence of $h(t)$ on G-CSF conc. and cellularity of PMC	η	0.88/pM	Opt	(11)
		H	0.05/h	Calc	(11)
		n_h	16	Opt	(11)
		d	0.1	Opt	(11)
	Parameters of dependence of x_1 on G-CSF conc.	α_1	0.1/h	Opt	(1)
		λ_1	10.694/h	Opt	(1)

Table 3 (*continued*)

Compartment	Description	Notation	Const. Value (Range)	Type	[Reference]/ (Equation)
		u_1	0.685	Opt	(1)
		G_1	1000 pM	Opt	(1)
	Parameters for dependence of $x_2$on G-CSF conc.	α_2	0.02/h	Opt	(2)
		λ_2	2.9/h	Opt	(2)
		u_2	0.58	Opt	(2)
		X_p	1000 pM	Opt	(2)
	Parameters for dependence of w_4 on x_1 and x_2	μ_1	8.4 steps/h	Opt	(9)
		m_1	1.2	Opt	(9)
		X_1	173 pM	Opt	(9)
		μ_2	3.6 steps/h	Opt	(9)
		m_2	1	Opt	(9)
		X_2	3.5 pM	Opt	(9)
		W_4^*	−1.26 steps/h	Calc	(9)
	Maturation steps number	n_4	95 steps	Opt	(6)
Blood	PMN turnover	α_b	0.091/h	Lit	[Dancey et al., 1976], [Cartwright et al., 1964], (A.10)
G-CSF	Endogenous production rate of G-CSF	Prod	4.83 pM/h (1–10)	Calc	[Shimazaki, 1995], (24)
	Receptor association rate	k_1	0.015/(pM h)	Lit	[Kuwabara, 1996b], (24)
	Non-specific clearance rate	α_G	0.06/h (0.01–0.5)	Calc	[Shimazaki, 1995], (24)
	Absorption rate from SC injection site	α_{abs}	0.208/h (0.01–0.5)	Calc	[Shimazaki, 1995], (24)
	G-CSF receptor production rate	ν	80 rec/h cell	Opt	(24)

References

Brent, R.P., 1973. Algorithms for Minimization Without Derivatives. Prentice-Hall, Englewood Cliffs, NJ.

Cartwright, G.E., Athens, J.W., Wintrobe, M.M., 1964. The kinetics of granulopoiesis in Normal man. Blood 24, 780–803.

Chatta, G.S., Price, T.H., Allen, R.C., Dale, D.C., 1994. Effects of in vivo recombinant methionyl human granulocyte colony-stimulating factor on the neutrophil response and peripheral blood colony-forming cells in healthy young and elderly adult volunteers. Blood 84, 2923–2929.

Cowling, G.J., Dexter, T.M., 1994. Apoptosis in the haemopoietic system. Philos. Trans. Roy. Soc. London 345, 257–263.

Dancey, J.T., Deubelbeiss, K.A., Harker, L.A., Finch, C.A., 1976. Neutrophil kinetics in man. J. Clin. Invest. 58, 705–715.

Dong, F., Liu, X., de Koning, J.P., Touw, I.P., Hennighausen, L., Larner, A., Grimley, P.M., 1998. Stimulation of Stat5 by granulocyte colony-stimulating factor (G-CSF) is modulated by two distinct cytoplasmic regions of the G-CSF receptor. J. Immunol. 161, 6503–6509.

Dong, F., Qiu, Y., Yi, T., Touw, I.P., Larner, A.C., 2001. The carboxyl terminus of the granulocyte colony-stimulating factor receptor, truncated in patients with severe congenital neutropenia/acute myeloid leukemia, is required for SH2-containing phosphatase-1 suppression of Stat activation. J. Immunol. 167, 6447–6452.

Dormer, P., Hultner, L., Mergenthaler, H.G., 1990. Proliferation and maturation of human bone marrow cells in infectious diseases. Pathol. Res. Pract. 186, 145–149.

Fliedner, T.M., Tibken, B., Hofer, E.P., Paul, W., 1996. Stem cell responses after radiation exposure: a key to the evaluation and prediction of its effects. Health Phys. 70, 787–797.

de Haas, M., Kerst, J.M., van der Schoot, C.E., Calafat, J., Hack, C.E., Nuijens, J.H., Roos, D., van Oers, R.H., von dem Borne, A.E., 1994. Granulocyte colony-stimulating factor administration to healthy volunteers: analysis of the immediate activating effects on circulating neutrophils. Blood 84, 3885–3894.

Harrison, W.J., 1962. The total cellularity of the bone marrow in man. J. Clin. Pathol. 15, 254–259.

Hoffman, R. (Ed.), 2000. Hematology, Basic Principles and Practice. Churchill Livingstone.

Irvine, A.E., Magill, M.K., Somerville, L.E., McMullin, M.F., 1998. Spontaneous intramedullary apoptosis is present in disorders other than myelodysplasia. Exp. Hematol. 26, 435–439.

Iwasaki, H., Shimoda, K., Okamura, S., Otsuka, T., Nagafuji, K., Harada, N., Ohno, Y., Miyamoto, T., Akashi, K., Harada, M., Niho, Y., 1999. Production of soluble granulocyte colony-stimulating factor receptors from myelomonocytic cells. J. Immunol. 163, 6907–6911.

Kuramoto, K., Follmann, D.A., Hematti, P., Sellers, S., Agricola, B.A., Metzger, M.E., Donahue, R.E., von Kalle, C., Dunbar, C.E., 2004. Effect of chronic cytokine therapy on clonal dynamics in nonhuman primates. Blood 103, 4070–4077.

Kuwabara, T., Kobayashi, S., Sugiyama, Y., 1996a. Pharmacokinetics and pharmacodynamics of a recombinant human granulocyte colony-stimulating factor. Drug Metab. Rev. 28, 625–658.

Kuwabara, T., Kobayashi, S., Sugiyama, Y., 1996b. Kinetic analysis of receptor-mediated endocytosis of G-CSF derivative, nartograstim, in rat bone marrow cells. Am. J. Physiol. 271, E73–E84.

Liu, X.W., Tang, Z.M., 1997. Pharmacokinetics of recombinant human granulocyte colony-stimulating factor in rabbits and mice. Zhongguo Yao Li Xue Bao 18, 44–48.

Liu, Y.K., Kosfeld, R.E., Koo, V., 1983. Marrow neutrophil mass in patients with non-hematological tumor. J. Lab. Clin. Med. 101, 561–569.

MacDonald, N., 1989. Biological Delay Systems: Linear Stability Theory. Cambridge University Press, Cambridge, UK, pp. 1–5.

Mackey, M.C., 1997. Mathematical models of hematopoietic cell replication and control. In: Othmer, H.G. (Ed.), The Art of Mathematical Modeling: Case Studies in Ecology, Physiology and Biofluids. Prentice Hall, Englewood Cliffs, NJ.

Mackey, M.C., Aprikyan, A.A., Dale, D.C., 2003. The rate of apoptosis in post-mitotic neutrophil precursors of normal and neutropenic humans. Cell Proliferat. 36, 27–34.

Mary, J.Y., 1984. Normal human granulopoiesis revisited. Biomed. Pharmacother. 38, 33–43, 66–77.

McLemore, M.L., Grewal, S., Liu, F., Archambault, A., Poursine-Laurent, J., Haug, J., Link, D.C., 2001. STAT-3 activation is required for normal G-CSF-dependent proliferation and granulocytic differentiation. Immunity 14, 193–204.

Ogawa, T., Kitagawa, M., Hirokawa, K., 2000. Age-related changes of human bone marrow: a histometric estimation of proliferative cells apoptotic cells, T cells, B cells and macrophages. Mech. Ageing Dev. 117, 57–68.

Ostby, I., Rusten, L.S., Kvalheim, G., Grottum, P., 2003. A mathematical model of reconstitution of granulopoiesis after high dose chemotherapy with autologous stem cell transplantation. J. Math. Biol. 47, 101–136.

Press, W.H., Flaunery, B.P., Teukolsky, S.A., Vetterling, W.T., 1993. Numerical Recipes in C: The Art of Scientific Computing. Cambridge University Press, Cambridge, UK.

Price, T.H., Chatta, G.S., Dale, D.C., 1996. Effect of recombinant granulocyte colony-stimulating factor on neutrophil kinetics in normal young and elderly humans. Blood 88, 335–340.

Rahman, Z., Esparza-Guerra, L., Yap, H.Y., Fraschini, G., Bodey, G., Hortobagyi, G., 1997. Chemotherapy-induced neutropenia and fever in patients with metastatic breast carcinoma receiving salvage chemotherapy. Cancer 79, 1150–1157.

Rolston, K., 2000. Prediction of neutropenia. Int. J. Antimicrob. Agents 16, 113–115.

Rubinow, S.I., Leibowitz, J.L., 1975. A mathematical model of neutrophil production and control in normal man. J. Math. Biol. 1, 187–225.

Schmitz, S., Loeffler, M., Jones, J.B., Lange, R.D., Wichmann, H.E., 1990. Synchrony of bone marrow proliferation and maturation as the origin of cyclic haemopoiesis. Cell Tissue Kinet. 23, 425–441.

Schmitz, S., Franke, H., Brusis, J., Wichmann, H.E., 1993. Quantification of the cell kinetic effect of G-CSF using a model of human granulopoiesis. Exp. Hematol. 21, 755–760.

Shimazaki, C., Uchiyama, H., Fujita, N., Araki, S., Sudo, Y., Yamagata, N., Ashihara, E., Goto, H., Inaba, T., Haruyama, H., 1995. Serum levels of endogenous and exogenous granulocyte colony-stimulating factor afterautologous blood stem cell transplantation. Exp. Hematol. 23, 1497–1502.

Shinjo, K., Takeshita, A., Ohnishi, K., Ohno, R., 1995. Expression of granulocyte colony-stimulating factor receptor increases with differentiation in myeloid cells by a newly-devised quantitative flow-cytometric assay. Br. J. Haematol. 91, 783–794.

Shochat, E., Stemmer, S.M., Segel, L., 2002. Human haematopoiesis in steady-state and following intense perturbations. Bull. Math. Biol. 64, 861–886.

Siewert, E., Muller-Esterl, W., Starr, R., Heinrich, P.C., Schaper, F., 1999. Different protein turnover of interleukin-6-type cytokine signalling components. Eur. J. Biochem. 265, 251–257.

Steinbach, K.H., Schick, P., Trepel, F., Raffler, H., Dohrmann, J., Heilgeist, G., Heltzel, W., Li, K., Past, W., van der Woerd-de Lange, J.A., Theml, H., Fliedner, T.M., Begemann, H., 1979. Estimation of kinetic parameters of neutrophilic, eosinophilic, and basophilic granulocytes in human blood. Blut 39, 27–38.

Steinbach, K.H., Raffler, H., Pabst, G., Fliedner, T.M., 1980. A mathematical model of canine granulopoiesis. J. Math. Biol. 10, 1–12.